Earthq Eng & Eng Vib (2018) 17: 311-324 **DOI**: https://doi.org/10.1007/s11803-018-0443-z

Behavior of braced excavation in sand under a seismic condition: experimental and numerical studies

Sanku Konai†, Aniruddha Sengupta‡ and Kousik Deb§

Department of Civil Engineering, Indian Institute of Technology Kharagpur, Kharagpur 721302, India

Abstract: The behavior of braced excavation in dry sand under a seismic condition is investigated in this paper. A series of shake table tests on a reduced scale model of a retaining wall with one level of bracing were conducted to study the effect of different design parameters such as excavation depth, acceleration amplitude and wall stiffness. Numerical analyses using FLAC 2D were also performed considering one level of bracing. The strut forces, lateral displacements and bending moments in the wall at the end of earthquake motion were compared with experimental results. The study showed that in a post-seismic condition, when other factors were constant, lateral displacement, bending moment, strut forces and maximum ground surface displacement increased with excavation depth and the amplitude of base acceleration. The study also showed that as wall stiffness decreased, the lateral displacement of the wall and ground surface displacement increased, but the bending moment of the wall and strut forces decreased. The net earth pressure behind the walls was influenced by excavation depth and the peak acceleration amplitude, but did not change significantly with wall stiffness. Strut force was the least affected parameter when compared with others under a seismic condition.

Keywords: braced excavation; shake table test; seismic; FLAC 2D; displacement

1 Introduction

Deep excavation in a congested urban area is often required for the construction of underground transport systems, basements of high-rise buildings, utility pipelines, etc. These excavations are often done vertically beneath the ground surface due to space constraints. Their retaining walls are constructed and supported at different levels by horizontal beams (struts) spanning between the two opposite sides of an excavation to laterally support near-vertical excavated faces. In temporary cases, these retaining walls are often just sheet pile walls, but reinforced concrete walls are used when they become part of the permanent structure being constructed. Figure 1 shows a schematic diagram of the typical braced excavation system considered in this study. As the excavation progresses, the retaining walls' lateral deflections need to be controlled, as they can induce adjacent ground surfaces to settle (Boscardin and Cording, 1989) and cause damage to nearby structures.

A significant number of numerical and experimental studies have been performed to understand the behavior of braced excavation under a static condition. Most of these studies are based either on finite element methods (Bose and Som, 1998; Carrubba and Colonna, 2000; Costa *et al*., 2007; Day and Potts, 1993; Finno and Harahap, 1991; Finno *et al*., 1991; His and Small, 1993; Hsiung, 2009; Karlsrud and Andresen, 2005; Ng *et al*., 1998; Ou and Hsieh, 2011; Yoo and Lee, 2008; Zdravkovic *et al*., 2005) or on database records of deep excavations in different types of soil from worldwide case histories (Finno *et al*., 2015; Hsieh and Ou, 1998; Kung *et al*., 2007; Liu *et al*., 2005; Long, 2001; Moormann, 2004; Tan and Wang, 2013a, b; Tanaka, 1999; Wang *et al*., 2005, 2010; Whittle *et al*., 2015). The static behavior of braced excavation has also been studied extensively with the help of laboratory model tests (Chowdhury *et*

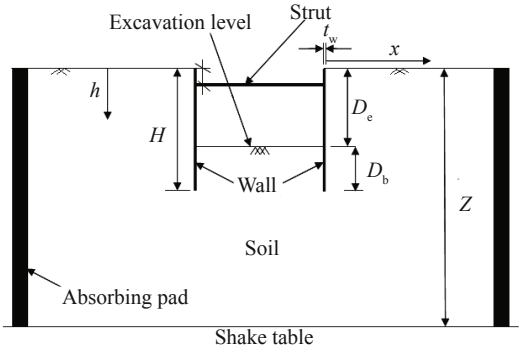

Fig. 1 Schematic diagram of braced excavation

Correspondence to: Kousik Deb, Department of Civil Engineering, Indian Institute of Technology Kharagpur, Kharagpur 721302, India
Tel: +91-3222-283434
E-mail: kousik@civil.iitkgp.ernet.in
†Research Scholar; ‡Professor; §Associated Professor

Received March 8, 2016; **Accepted** August 26, 2016

al., 2016; Georgiadis and Anagnostopoulos, 1999; Nakai *et al*., 1999; Takemura *et al*., 1999; Tefera *et al*., 2006). However, studies on braced retaining walls under a seismic condition are very limited. Callisto *et al*. (2008) performed numerical analyses of this type of wall, finding that as a seismic wave propagated through the soil it quickly mobilized shear forces in the soil adjacent to the propped cantilever wall, causing—when compared with the static condition—a significant increase in bending moment and lateral displacement in the wall as well as an increase in axial forces in the struts. Callisto and Soccodato (2010) performed a numerical analysis of flexible, embedded cantilever retaining walls in a dry, coarse-grained soil using FLAC and two earthquakes histories. They observed that the seismic resistance to the permanent rigid body movement of a retaining wall could be expressed in terms of critical horizontal acceleration, which was calculated by an iterative method based on limit equilibrium. They also found that the bending moment was large during an earthquake due to instantaneous contact-stress distribution. Conti *et al*. (2010) conducted dynamic centrifuge tests on reduced-scale models of cantilevered retaining walls. They observed that the permanent displacements (during shaking) and residual bending moments (after shaking) depended not only on the entire acceleration time history but also on present earthquake intensity. Conti *et al*. (2012) performed several centrifuge tests on cantilever and propped cantilever retaining walls in dry sand. They observed that no significant additional displacement occurred during an earthquake if the retaining wall had already experienced an earthquake that was more severe than the present one. They also observed that the retaining wall experienced nearly rigid permanent displacements for maximum accelerations that were smaller than the critical limit equilibrium value. The stability of a braced excavation and nearby ground surface depended primarily on the number, stiffness, and vertical and horizontal spacing of the struts and on the stiffness and embedment depth of the retaining wall (Chowdhury *et al*., 2013). Chowdhury *et al*. (2015) investigated the behavior of a strutted retaining structure under a seismic condition by performing numerical analysis. Their observed results showed that during an earthquake the displacement of the wall was the most affected and the axial force on the strut was the least affected parameter.

In addition to the above studies, a number of numerical studies have been performed on retaining walls, gravity walls, cantilever walls, anchored walls and mechanically stabilized earth retaining walls under a seismic condition (Caltabiano *et al*., 2000; Frawley, 1992; Gazetas *et al*., 2004; Ling *et al*., 2005b; Madabhushi and Zeng, 1998, 2008; Neelakantan *et al*., 1992; Psarropoulos *et al*., 2005; Richards *et al*., 1999; Siller and Frawley, 1992; Yogendrakumar *et al*., 1992; Veiskarami *et al*., 2015; Wartman *et al*., 2006). Hsiung (2009) observed from numerical analysis that the most sensitive parameters for a retaining wall were the normal stiffness (Kn) and shear stiffness (Ks) of the interface between the soil and the wall. Hsieh *et al*. (2013) found that lateral wall deflection was reduced after the installation of cross walls. Experimental studies have also been conducted to investigate the behavior of these different types of walls under a seismic condition (Atik and Sitar, 2010; Ling *et al*., 2005a, 2009; Tufenkjian and Vucetic, 2000; Watanabe *et al*., 2003; Zeng, 1998).

As may be seen from the above discussion, a very limited number of studies have been conducted on the behavior of braced retaining walls under a seismic condition. The primary reason for this insufficiency is that these types of construction are usually temporary in nature. However, now-a-days, many metro construction projects continue for 6 to 7 years, necessitating that these underground support systems be designed for an earthquake condition, especially in earthquake-prone zones.

In this study, a small-scale model study in the laboratory and corresponding numerical analyses were performed to investigate the behavior of a braced retaining wall with a single bracing or strut under sinusoidal loads in dry sand. The effects studied were the excavation depth, peak acceleration amplitude and stiffness of the retaining wall on the performance of the system in terms of forces in the struts, moments developed in the wall, deflection of the wall, displacement of the adjacent ground surface and lateral earth pressure distribution behind the walls due to seismic loading.

2 Laboratory model tests

The model tests of the braced excavation were done using small-scale models in the laboratory. The use of scaled models in geotechnical engineering offers the advantage of simulating complex systems in a controlled laboratory environment and the opportunity to gain insight into the fundamental mechanisms governing the behavior of these systems. The model tests were conducted in a 1-g environment.

A physical model of a braced wall system was constructed and tested under dynamic loading. A braced wall system consisting of one level of strut was modeled by two 880 mm long, 2.4 mm thick (t_w) and 200 mm high (H) plexiglass walls. The density and the modulus of elasticity of the plexiglass were 1010 kg/m^3 and 6.3×10^9 Pa, respectively. A 160 mm horizontal gap (B) was maintained between the two model walls by two rectangular horizontal beams or struts located at 40 mm (s) below the top of the walls. It is well documented that the behavior of a braced wall can be influenced by the location of the struts (Callisto and Soccodato, 2007); therefore, a 440 mm horizontal spacing was maintained between the two struts. The struts were also made of plexiglass and had a cross-sectional area of 1.44×10^{-4} m^2. The struts were screwed to the two walls. The moments

from the walls were not transferred to a strut, which was designed as an axial load-carrying member. A number of strain gauges were glued to the surface of the walls and struts (as shown in Fig. 2), so that strains developed in these members during a shake table test could be measured and deformations and bending moments in these members could be calculated. The axial forces in the struts were also calculated from the readings of the strain gauges attached to the struts. In addition, two linear variable differential transformers (LVDTs) were attached to the walls to measure their deflections at specific depths. To obtain a measurable amount of lateral deformation of the wall, higher values of D_e/H (where D_e is the depth of the excavation and H is the height of the wall) were used to determine trends. However, these higher values may not be practical. Various numerical studies and similar small-scale model tests with one strut and higher D_e/H have been conducted by researchers (Callisto, 2014; Callisto and Soccodato, 2009; Callisto *et al*., 2008; Conti *et al*., 2012).

The experimental setup (as shown in Fig. 3) consisted of a shake table, which was essentially a 1m x 1m steel table mounted on rails. The load-carrying capacity of the table was 5 ton. The table was attached to an actuator that vibrated the table in a uniaxial horizontal direction. The servo hydraulic actuator had a capacity of +/- 50 kN and a stroke length of +/-100 mm. The actuator was driven by a controller that had the capability to accept actual earthquake loading (random, cyclic) as input and

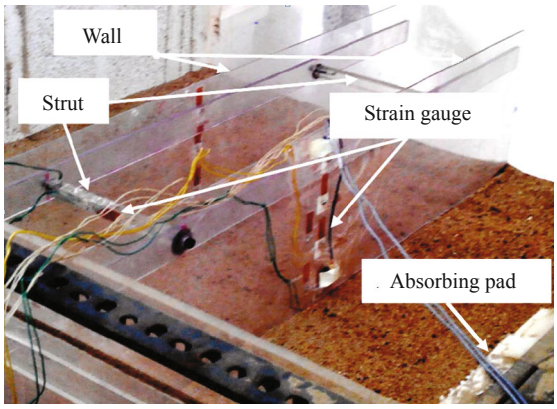

Fig. 2 Model braced walls within the test tank

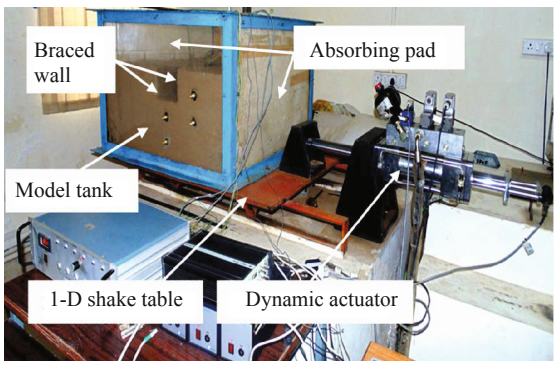

Fig. 3 Test setup of laboratory experiment

generated a frequency in the range of 0.01 Hz to 25 Hz. The actuator had the capacity to hold and restart loading during a test and the facility to increase the base load, frequency and amplitude during a test.

The model tests, reported here, were performed in a rigid plexiglass box with an open top of dimensions 0.88 m × 0.8 m × 0.6 m (length × breadth × height). The plexiglass sheets were 16 mm thick and glued to each other as well as fixed in a steel frame consisting of steel angles as shown in Fig. 3. Lombardi *et al*. (2015) observed that the use of an absorbing pad with soft material in the boundaries can significantly absorb energy at the boundaries. Thus, in the present study, thermocols with 32 mm thickness were placed as absorbing pads on three sides of the box and the glass on the fourth side was lightly lubricated with grease to reduce side friction and the reflection and refraction of waves at the ends. The test chamber was filled up to a depth of 400 mm (Z) with dry sand, maintaining a uniform density of 1600 kg/m^3 (unit weight = 15.7 kN/m^3). The process of sand filling and compaction was done in four layers, with the thickness of each layer being 100 mm. Since the seismic effect on a braced excavation is the subject of the present study, the actual construction sequence of a braced excavation was not performed. Instead, the walls with the struts between them were placed in the middle of the tank once the tank was filled with sand up to the specified depth, and then the sand-filling operation of the test tank was resumed. In this study, the depths of the embedment of the walls (D_b) and the depth of the excavation (D_e) between the two walls was varied between 40-100 mm and 100-160 mm, respectively, in order to study their influence on the performance of a braced excavation during shaking. Two accelerometers, one near the ground surface and another near the excavation level, were placed into the soil; a third accelerometer was placed on the shake table.

The dry sand utilized in the shake table tests was obtained locally from a river and is referred to as "Kasai River sand." The grain-size distribution of the sand is shown in Fig. 4. It is classified as poorly graded sand (SP), according to the Unified Soil Classification System (USCS). The specific gravity of the sand is 2.67. The maximum dry unit weight γ_d(max) is 16.7 kN/m^3, and the minimum dry unit weight γ_d(min) is 14.03 kN/m^3. The uniformity coefficient (c_u) and coefficient of curvature (c_c) of the sand were found to be 2.84 and 0.87, respectively. In the model tests, the bulk unit weight of the sand was maintained at 15.7 kN/m^3 (1600 kg/m^3 bulk density) and a relative density D_r of 67%. Consolidated drained triaxial tests were conducted on saturated Kansai River sand to obtain effective soil strength parameters for numerical analysis. The effective cohesion (c') and the effective angle of friction (ϕ') obtained from triaxial tests were 0.0 kPa and 38°, respectively. Table 1 shows the material properties of the foundation sand. The coefficient of lateral earth pressure for the soil was calculated using the well-known formula K_h = 1-sinϕ', which yielded a value of 0.38 for the soil.

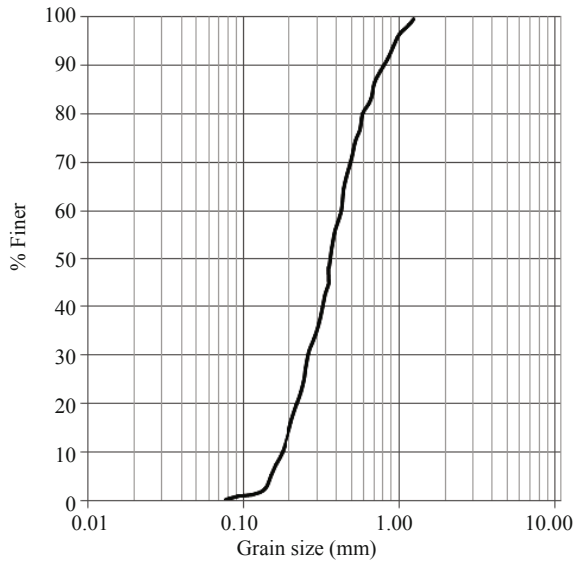

Fig. 4 Grain size distribution of Kasai River sand

Table 1 Geotechnical parameters of the soil

Properties	Value
Mass density (kg/m^3)	1600
Cohesion (Pa), c'	0
Angle of internal friction, ϕ'	38^o
Dilation angle, Ψ	8^0
Poisson's ratio, μ_s	0.3

In the shake table tests, instead of actual earthquake motions, sinusoidal motions of specified amplitude, frequency and number of cycles were applied so that the effect of these parameters on the braced excavation could be studied. In the present study, the performance of the braced excavation during 14 cycles of sinusoidal motions with peak amplitudes between 0.3 g and 0.4 g at 2 Hz frequency were studied. Figure 7(a) shows a typical input motion specified during the present study. In the shake table tests, the depth of excavation between the walls, stiffness of the model walls and amplitude of the input acceleration were varied, so that their effect on the braced excavation under a seismic condition could be studied. Table 2 shows the different cases studied.

3 Numerical modeling

Two-dimensional (plane strain) finite difference analyses of the braced excavation were performed using the commercial software FLAC 2D (Itasca, 2005). Each of the two 200 mm-high and 2.4 mm-thick braced walls was discretized by 10 two-dimensional beam elements. At each node, the beam element had three degrees of freedom (two displacements and one rotation). The beam elements were assumed to be elastic. The strut between the two retaining walls was also modeled by a beam element. The connections between the walls and the strut were assumed to be pin-jointed, i.e., with no moment transfer possible through the joints. For the present plane strain analyses, Young's modulus of the walls was calculated using $E_p = E/(1-\mu^2)$ (Itasca, 2005), where Young's Modulus of the plexiglass (E) and the Poisson ratio (μ) were taken as 6.3×10^9 N/m^2 and 0.35, respectively.

The foundation soil (800 mm × 400 mm) within which the braced walls were located was discretized by 40 × 20 numbers of quadrilateral elements of size 20 mm × 20 mm. For the dynamic analyses, absorbing boundaries were assumed on the two sides (as in the experiment, absorbing pads were used to absorb energy at the boundaries). As in the model experiment, 14 cycles of sinusoidal waves of amplitude 0.35 g were applied at the bottom of the numerical model. The frequency of the motion was 2 Hz in both the numerical and experimental model tests; the magnitude of the maximum acceleration varied between 0.3 g and 0.4 g. A schematic diagram illustrating the numerical model and the boundary conditions is shown in Fig. 5.

Under a plane-strain condition, the shear stress (τ) and the shear strain (γ_s) (Itasca, 2005) were related as

$$\frac{\tau}{G_0} = \frac{G_s(\gamma_s)}{G_0}\gamma_s = M_s(\gamma_s).\gamma_s \tag{1}$$

where $G_s(\gamma_s)$ is the secant shear modulus that is a function of γ_s. G_0 is the small strain shear modulus and M_s is the normalized secant shear modulus. In the present analyses, it was assumed that the cyclic soil behavior could be represented by the relationship between M_s

Table 2 Shake table tests on braced excavation in dry sand

Test	D_e (mm)	D_b (mm)	D_e/H	s (mm)	t_w (mm)	Z (mm)	B (mm)	Maximum acceleration amplitude
BW1	100	100	0.5	40	2.4	400	160	0.35 g
BW2	140	60	0.7	40	2.4	400	160	0.35 g
BW3	160	40	0.8	40	2.4	400	160	0.35 g
BW4	140	60	0.7	40	2.4	400	160	0.3 g
BW5	140	60	0.7	40	2.4	400	160	0.4 g
BW6	140	60	0.7	40	1.4	400	160	0.35 g

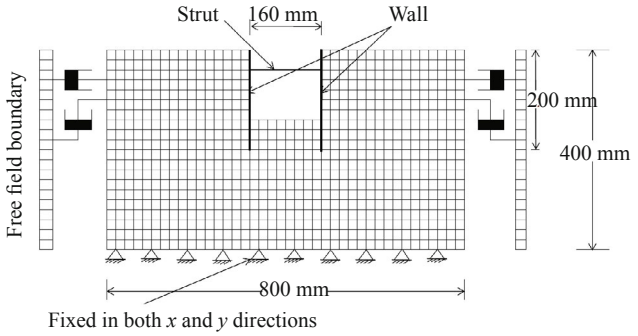

Fig. 5 Numerical discretization of the braced excavation in FLAC 2D analyses

and γ_s (Itasca, 2005). The modulus degradation and hysteretic damping material curves of Kasai River sand were specified for modeling the nonlinearity and shake down of strengths during dynamic loading using the "sigmoidal" model available in FLAC 2D. The sigmoidal curves were monotonic within the defined range and had the appropriate asymptotic behavior. The sigmoidal model in FLAC 2D is defined as:

$$M_s = y_0 + \frac{a}{1+\exp\left[-\left(L-x_0\right)/b\right]} \tag{2}$$

where L is the logarithmic strain, i.e., $L = \log_{10}(\gamma_s)$. The parameters a, b, x_0 and y_0 are the curve-fitting parameters for which the values are 0.96, -0.396, -1.16 and -0.0399, respectively, for Kasai River sand. Figure 6 compares the modulus degradation of the Kasai River sand as obtained from the cyclic triaxial tests and as estimated by FLAC 2D using the above equation. The simulation of the modulus degradation curve was reasonably close to the experimental results.

The soil-structure interaction was modeled by using both a shear and a normal spring at each node of the structure. The introduction of a normal spring modeled the behavior of the relative lateral motion between the wall and the surrounding soil, as they were of different stiffnesses. Similarly, the shear spring manifested the relative downward movement of the soil and the walls. The interface parameters, including the friction angle, normal and shear stiffness (K_n and K_s), were estimated from the drained friction angle (ϕ'), bulk modulus (K) and shear modulus (G) of the foundation soil. The normal and shear stiffnesses of the interface were selected so that the stiffness for each was approximately ten times the equivalent stiffness of the stiffest neighboring zone. The normal and shear stiffness (K_n and K_s) (Itasca, 2005) were estimated as

$$K_n = K_s = 10\max\left[\frac{(K+\frac{4}{3}G)}{\Delta z_{\min.}}\right] \tag{3}$$

where $\Delta z_{\min.}$ is the smallest width (20 mm) of the adjoining zone in the normal direction to the interface. The shear modulus (G) and the bulk modulus (K) of the soil were calculated as $G = E_s/2(1+\mu_s)$ and $K = E_s/3(1-2\mu_s)$, where μ_s is the Poisson's ratio of the surrounding soil.

The normal and shear stiffness (K_n and K_s) considered for the numerical study was 2.9×10^9 Pa/m. The interface friction angle between the plexiglass structure and the sand was 20^0. The coefficient of lateral earth pressure for the soil was calculated using the well-known formula $K_h = 1\text{-}\sin\phi'$, which yielded a value of 0.38 for the sand. The Young's modulus of the soil used in the numerical analysis was determined from Eq. 4 (Janbu, 1963):

$$E_s = P_{ref} K_d \left[\frac{(\sigma_c)}{P_{ref}}\right]^n \tag{4}$$

where P_{ref} =100 kPa, σ_c = confining pressure (varies with the depth of the soil). K_d and n are two parameters that were found to be 402 and 0.5, respectively, from the laboratory drained compression triaxial tests on Kasai River sand. Table 3 summarizes the other model parameters utilized in the numerical analyses of the braced excavation under a dynamic loading condition.

In the present study, the mesh size was taken as 0.02 m×0.02 m. The maximum frequency that could be modeled for smooth wave propagation through all elements depended on the minimum value of G_0 (small strain shear modulus), which was obtained at the center of the top-most element of the model, i.e., at a depth of 0.02/2=0.01 m below ground level. The value of G_0 was found to be 377.65 kPa. The shear wave speed (C_s), and the maximum frequency (f_{max}) that could be modeled, were calculated from the following equations (Itasca, 2005):

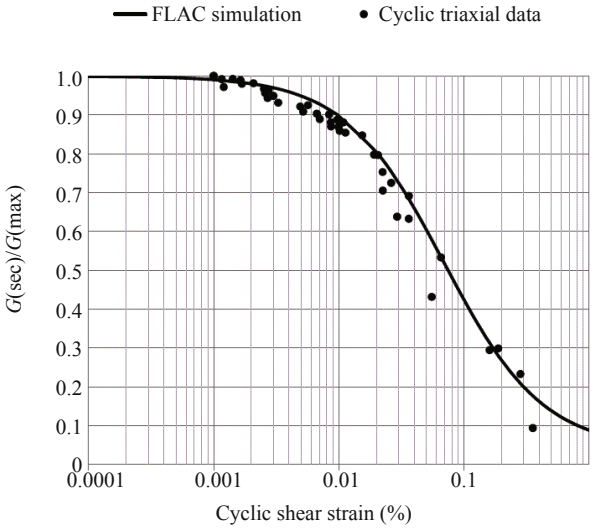

Fig. 6 Modulus reduction curve for Kasai River sand

Table 3 Model parameters used for the numerical analyses (FLAC) of braced excavation

Density of soil (kg/ m^3)	Friction angle (ϕ') (Degree)	Dilation angle (ψ)	Poisson's ratio (μ_s) of soil	Braced wall (EI) (N·m^2/m)	Strut (EA) (N/m)
1600	38^0	8^0	0.3	7.29	9.12×10^5

$$C_S = \sqrt{\frac{G_0}{\rho}} \tag{5}$$

$$f_{max} = \frac{C_S}{\lambda} \tag{6}$$

The value of C_s is 15.36 m/s. λ, the wavelength associated with the highest frequency component that contains appreciable energy. The wavelength was calculated (Itasca, 2005) as

$$\lambda = 10\Delta l \tag{7}$$

where Δl is the spatial element size, i.e., 0.02 m. The value of f_{max} is 76.8 Hz, i.e., the maximum frequency with which the wave can propagate through the model. For all seismic events, the input frequency was very low (i.e., 2 Hz), which allowed smooth propagation of the wave though the soil media.

4 Results and discussion

During shake table tests on the embedded braced walls with one level of strut in dry sand, the amplification of ground motions, strains in the wall and the strut were measured. The bending moments and the displacements of the walls were obtained indirectly from the measured strains on the wall. The displacements of the wall were also measured at two elevations by LVDTs. To measure the horizontal acceleration time history during shaking, accelerometers were placed on the shake table at the bottom of the excavation and at the top of the soil surface behind the walls. As may be seen from Figs. 7(a-c), the peak ground motion amplified by 1.27 times at the bottom of the excavation and by 1.44 times at the top of the ground level behind the walls, as recorded by accelerometers for 7 seconds of sinusoidal input motions of 0.35 g at 2 Hz applied at the bottom. Six strain gauges were attached to one of the walls at different elevations from the top. Additionally, two LVDTs are also attached at 15 mm and 80 mm, respectively, from the top of the wall. The bending moments developed in the wall during the application of the motions were back-calculated from strain-gauge readings. LVDT readings were used to obtain the lateral displacements of the entire wall by double-integrating the strain-gauge data. The axial loads on the strut or strut forces, F, were also evaluated during the tests from readings of the strain gauges attached to the struts. The bending moments, M, the lateral displacements, u, of the wall and the strut forces thus obtained were compared with those predicted from the numerical analyses. Different influencing parameters such as excavation depth, peak acceleration amplitude and wall stiffness were varied to understand the behavior

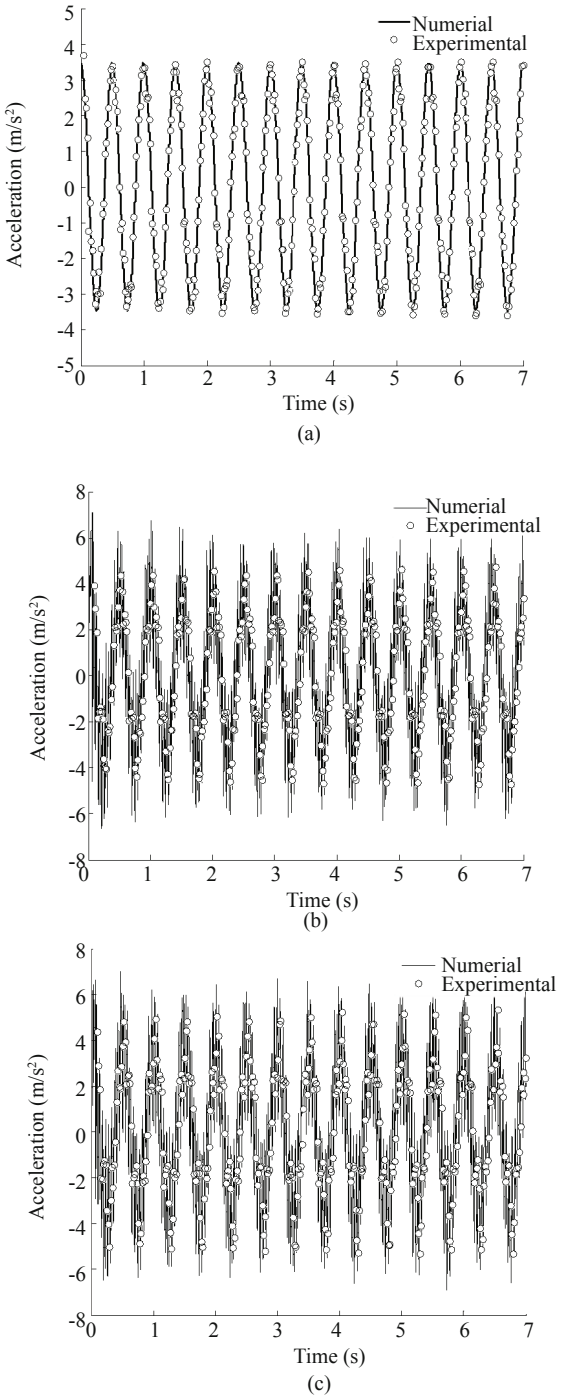

Fig. 7 Acceleration time history in the model test BW2 recorded (a) at the shake table (b) at the bottom of excavation (D_e/H=0.7) and (c) at the top of the soil behind the wall

of a braced wall during a seismic event. The width of the excavation, B, between the two walls was kept at a constant 160 mm for all of the cases mentioned in Table 2, as excavation width can influence the behavior of a braced wall (Callisto and Soccodato, 2007). In addition to the above, ground surface displacement, v, and lateral earth pressures behind the walls were also obtained from the numerical analysis.

The results obtained from the laboratory shake table tests and the numerical analyses are presented in non-dimensional forms. The post-seismic results presented here are due to applied seismic events only. The values of the lateral displacement for the wall, u, were normalized with respect to the excavation depth, D_e. The bending moment in the wall, M, was normalized with respect to γH^3, where γ is the unit weight of the sand. The depth from the ground surface, h, and the horizontal distance from the right wall to the right boundary, x (as shown in Fig. 1), were also normalized with respect to H. The excavation depth, D_e was normalized with respect to the total depth of the wall, H. The axial forces in the struts were also presented by normalizing them with respect to EA, where E is the Young's modulus of the strut material and A is the cross-section area of the strut.

The influence of parameters such as depth of excavation, peak acceleration applied at the base and wall stiffness on the wall's maximum non-dimensional lateral displacement, u/D_e, are presented in Table 4. The lateral displacement, u/D_e, along the normalized depth of the wall, h/H, is also presented in Figs. 8(a-c) for different normalized excavation depths, D_e/H, peak acceleration and wall stiffness. The same peak acceleration amplitude of 0.35 g, and the same wall stiffness of 7.29 N·m^2/m, were chosen for all of the test results shown in Fig. 8(a). Tests were conducted under different D_e/H values of 0.5, 0.7 and 0.8. For test results presented in Fig. 8(b), the same D_e/H = 0.7 and wall stiffness = 7.29 N·m^2/m were used, but acceleration amplitude was varied as 0.3 g, 0.35 g and 0.4 g. Similarly, the same acceleration amplitude of 0.3 g and D_e/H = 0.7 were selected for all of the test results presented in Fig. 8(c). However, the stiffness values of 7.29 N·m^2/m and 1.45 N·m^2/m were used for higher-wall stiffness and lower-wall stiffness, respectively.

Based on centrifuge test results, Conti *et al*. (2012) presented that for D_e/H = 0.7 in a propped retaining wall, the lateral displacement of the wall toe was about 0.5 -1% of the total depth of the retaining wall. In the present study, the lateral displacement of the braced wall toe was

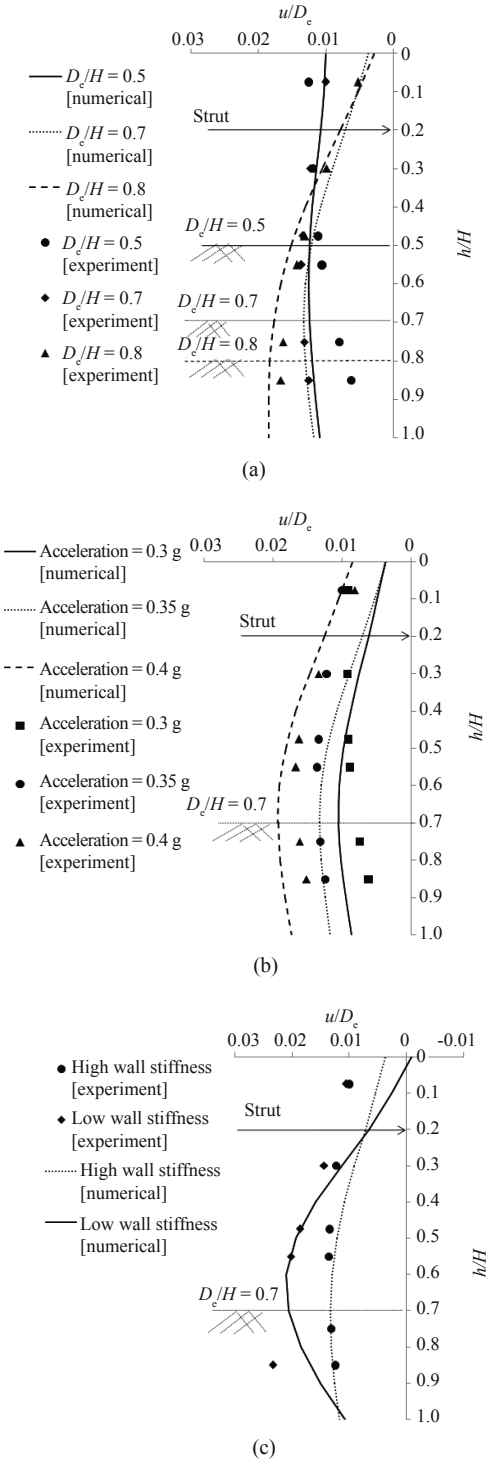

Fig. 8 Lateral displacements of the braced wall for (a) different excavation depths (D_e/H), (b) different peak amplitudes of input acceleration, and (c) different wall stiffnesses

Table 4 Influence of depth of excavation, peak base acceleration and wall stiffness on the maximum non-dimensional lateral displacement (u/D_e) of the wall

Case	D_e/H			Peak acceleration (g)			Wall stiffness	
	0.5	0.7	0.8	0.3	0.35	0.4	High	Low
Numerical	0.0126	0.0133	0.0185	0.0105	0.0133	0.0193	0.0133	0.0210
Experiment	0.0126	0.0137	0.0167	0.0093	0.0137	0.0167	0.0137	0.0233

0.8% of the total depth of the wall (H) and thus conforms to the observations of Conti *et al*. (2012). Table 4 shows that the maximum value of u/D_e increased by 6% in the numerical analysis and 8% in the shake table test when D_e/H increased from 0.5 to 0.7. The maximum value of u/D_e increased by 39% in the numerical analysis and 22% in the model test when D_e/H increased from 0.7 to 0.8. Table 4 shows that the maximum value of u/D_e increased by 47% and 22% in the model test when peak acceleration increased from 0.3 g to 0.35 g and 0.35 g to 0.4 g, respectively. Table 4 also shows that the maximum value of u/D_e increased by 27% and 45% in the numerical analysis when peak acceleration increased from 0.3 g to 0.35 g and 0.35 g to 0.4 g, respectively. Similarly, when the wall stiffness decreased by 80%, the maximum value of u/D_e increased by 57% and 70% in the case of the numerical analysis and shake table test, respectively.

It may be further observed from Fig. 8(a) that as the excavation depth increased in a braced excavation with one level of strut, the location of the maximum lateral displacement occurred near the bottom of the excavation. A uniform lateral displacement was observed within the excavated portion of the wall with higher stiffness, but in case of the wall with lower stiffness more displacement was observed near the bottom of the excavation.

The normalized bending moment, $M/\gamma H^3$, along the depth, h/H, of the braced wall are shown in Figs. 9(a-c). The same peak acceleration amplitude of 0.35 g, and the same wall stiffness of 7.29 N·m^2/m, were chosen for all of the test results shown in Fig. 9(a). Tests were conducted under different D_e/H values of 0.5, 0.7 and 0.8. For the test results presented in Fig. 9(b), the same D_e/H = 0.7 and wall stiffness = 7.29 N·m^2/m were used, but the acceleration amplitude was varied as 0.3 g, 0.35 g and 0.4 g. Similarly, the same acceleration amplitude of 0.3g and D_e/H = 0.7 were selected for all of the test results presented in Fig. 9(c). However, the stiffness values of 7.29 N·m^2/m and 1.45 N·m^2/m were used for higher-wall stiffness and lower-wall stiffness, respectively. It may be seen from these figures that the maximum bending moment occurred near the excavation level or the strut level for all cases. The maximum bending moments, $M/\gamma H^3$, in the wall for different depths of excavation, peak amplitudes of base motion and wall stiffnesses during the cyclic motion are presented in Table 5. This table shows that the maximum value of $M/\gamma H^3$ increased by 127% and 13% in the numerical analysis as D_e/H increased from 0.5 to 0.7 and 0.7 to 0.8, respectively. Table 5 also shows that the maximum value of $M/\gamma H^3$ increased by 15% and 14% as per the numerical analysis when the peak amplitude of the base acceleration was increased from 0.3 g to 0.35 g and from 0.35 g to 0.4 g, respectively. On the other hand, the maximum value of $M/\gamma H^3$ decreased by 26% in the numerical analysis and 66% in the shake table test when the wall stiffness was decreased by 80%.

In the shake table experiments and the numerical analysis, only one level of strut or bracing at 40 mm from the top of the wall was used (as shown in Figs. 1 and 2). The normalized strut forces, F/EA, obtained from the model tests and the numerical analyses are presented in Table 6. It may be observed from this table that when D_e/H increased from 0.5 to 0.7 and from 0.7 to 0.8, F/EA increased in the numerical analyses by 26% and 5%, respectively. Similarly, when the peak amplitude of the base motion increased from 0.3 g to 0.35 g and from 0.35 g to 0.4 g, F/EA increased in the numerical analyses by 13% and 8%, respectively. When the wall stiffness decreased by 80%, the normalized strut force in both the numerical analysis and model tests decreased by 7% and 21%, respectively. Differences between the experimental and numerical results may be the result of model interface properties that were determined by FLAC guidelines in the numerical modeling. The model interface properties may not very accurately represent actual interface behavior. To determine actual interface properties by experiment is very difficult. Thus, the use of the nonlinear model, although very much accepted in geotechnical engineering, has some limitations in modeling complicated soil-structure interaction

Table 5 Maximum non-dimensional bending moment ($M/\gamma H^3$) in the right wall for different excavation depths, peak amplitudes of base motion and wall stiffnesses

Case	D_e/H			Peak acceleration (g)			Wall stiffness	
	0.5	0.7	0.8	0.3	0.35	0.4	High	Low
Numerical	0.0057	-0.0129	-0.0146	-0.0112	-0.0129	-0.0148	-0.0129	-0.0096
Experimental	-0.0073	-0.0079	-0.0118	-0.0076	-0.0079	-0.0131	-0.0079	-0.0027

Table 6 Normalized strut forces (F/EA) ($\times 10^{-5}$) with varying D_e/H, peak acceleration amplitudes and wall stiffnesses

Case	D_e/H			Peak acceleration (g)			Wall stiffness	
	0.5	0.7	0.8	0.3	0.35	0.4	High	Low
Numerical	5.16	6.53	6.83	5.77	6.53	7.06	6.53	6.08
Experimental	5.75	5.87	6.00	3.82	5.87	8.45	5.87	4.65

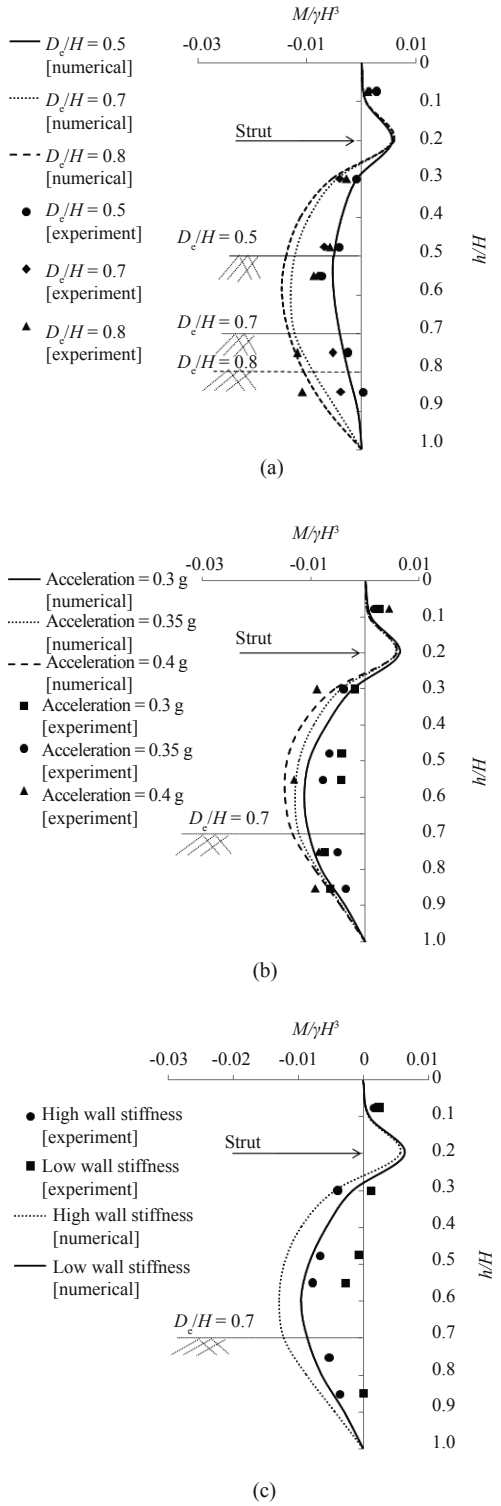

Fig. 9 Bending moments in the braced wall for (a) different excavation depths (D_e/H), (b) different peak amplitudes of input acceleration and (c) different wall stiffnesses

problems like the present one.

The total vertical displacement, v, of the ground surface behind the wall of the braced excavation was obtained from numerical analyses for different excavation depths, peak acceleration amplitudes and wall stiffnesses. The maximum ground surface displacements from the numerical analysis are shown in Table 7. In the table, the vertical displacement, v, is presented in a non-dimensional form, v/H. When D_e/H increased from 0.5 to 0.7 and from 0.7 to 0.8, v/H increased by 93% and 5%, respectively. When the peak acceleration amplitude increased from 0.3 g to 0.35 g and from 0.35 g to 0.4 g, v/H increased by 50% and 64%, respectively. A 66% increment in v/H value was observed when the wall stiffness decreased by 80%. Thus, it is observed that, within the selected parameters, the lateral displacement of the wall and vertical ground surface displacement were more affected than the bending moment in the wall or strut force due to the change in the peak acceleration applied at the base. A change in the stiffness of the wall affected the lateral displacement, bending moment of the wall and ground surface displacement more than strut force.

The total lateral earth pressures acting on the wall of the braced excavation were also obtained from the numerical analyses. The lateral earth pressure, σ_h, was normalized with respect to γH. The simulated lateral active earth pressures obtained from the numerical study at the end of the motions were compared with the theoretical lateral earth pressure (e.g., Coulomb earth pressures for the static and the Mononobe-Okabe method, or the M-O method in a seismic condition) as well as those pressures estimated by empirical or semi-empirical methods (e.g., Peck *et al*., 1974); these are presented in Fig. 10. In the numerical study, the lateral earth pressures were obtained for static and static-plus-seismic conditions (with an acceleration amplitude of 0.35 g) for one level of strut (at the top position) and three levels of strut (i.e., multi-strut) with a D_e/H= 0.7 and wall stiffness = 7.29 N·m²/m. The results show that Coulomb's theory and the Mononobe-Okabe method underestimated the lateral earth pressure when compared with the earth pressure obtained near the strut position of the wall from the numerical study for the static and seismic conditions, respectively. The method proposed by Peck *et al*. (1974) for multi-propped excavations in sandy soil overestimated the lateral earth pressure for a static condition obtained by theoretical methods as well as the numerical study. However, the earth pressure obtained from the numerical study under a seismic condition was more than the earth pressure proposed

Table 7 Maximum ground surface displacement (v/H) for different D_e/H, peak acceleration amplitudes and wall stiffnesses

D_e/H			Peak sinusoidal acceleration (g)			Wall stiffness (m)	
0.5	0.7	0.8	0.3	0.35	0.4	High	Low
0.00114	0.00220	-0.00221	-0.00147	0.00220	0.00360	0.00220	0.00364

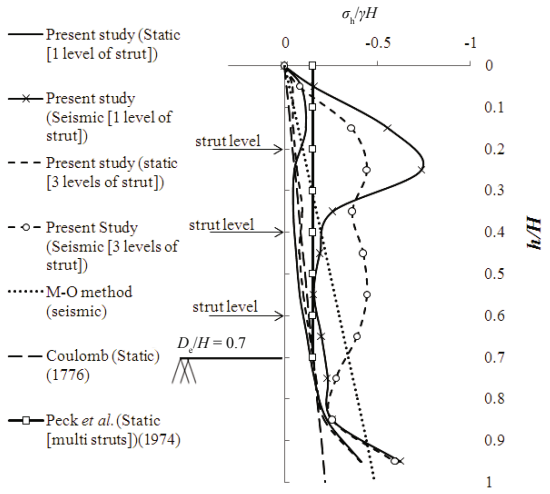

Fig. 10 Comparison of active earth pressure obtained from the present study with different established theories

by Peck *et al*. (1974). In addition, the numerical study showed that the maximum lateral earth pressure was greater in the one-strut case than in the multi-strut case under both the static and seismic conditions. Under the seismic condition, the earth pressure was greater near the strut level for the single-strut case, but for the multi-strut case (i.e., given three levels of struts), the earth pressure was fairly uniform throughout the excavation depth (except near ground level). The uniform seismic earth pressure obtained by the numerical study (with an acceleration amplitude of 0.35 g) for the multi-strut case was almost three times more than the uniform earth pressure (static) proposed by Peck *et al*. (1974) for multi-propped excavations in sandy soil.

The active and passive earth pressures at the end of the motions are shown in Figs. 11(a-c) for different excavation depths, peak acceleration amplitudes and wall stiffnesses. The earth pressures obtained for different conditions were also compared with the Mononobe-Okabe method. The same peak acceleration amplitude of 0.35 g, and the same wall stiffness of 7.29 N·m^2/m, were chosen for all of the test results shown in Fig. 11(a). The tests were conducted under different D_e/H values of 0.5, 0.7 and 0.8. For the test results presented in Fig. 11(b), the same D_e/H = 0.7 and wall stiffness = 7.29 N·m^2/m were used, but the acceleration amplitude was varied as 0.3 g, 0.35 g and 0.4 g. Similarly, the same acceleration amplitude of 0.3 g and D_e/H =0.7 were selected for all of the test results presented in Fig. 11(c). However, stiffness values of 7.29 N·m^2/m and 1.45 N·m^2/m were used for higher-wall stiffness and lower-wall stiffness, respectively. Figures 12 (a-c) show the net lateral earth pressures acting on the wall.

From Figs. 11(a-c) and Figs. 12(a-c), we may conclude that the excavation depth and the peak acceleration amplitude of the input motions had more influence than wall stiffness. The Mononobe-Okabe method underestimated the active earth pressure when compared to the earth pressure at the strut level obtained from the numerical study under a seismic condition. However, the Mononobe-Okabe method overestimated the passive earth pressure when compared to the passive earth pressure throughout the depth of the wall below the

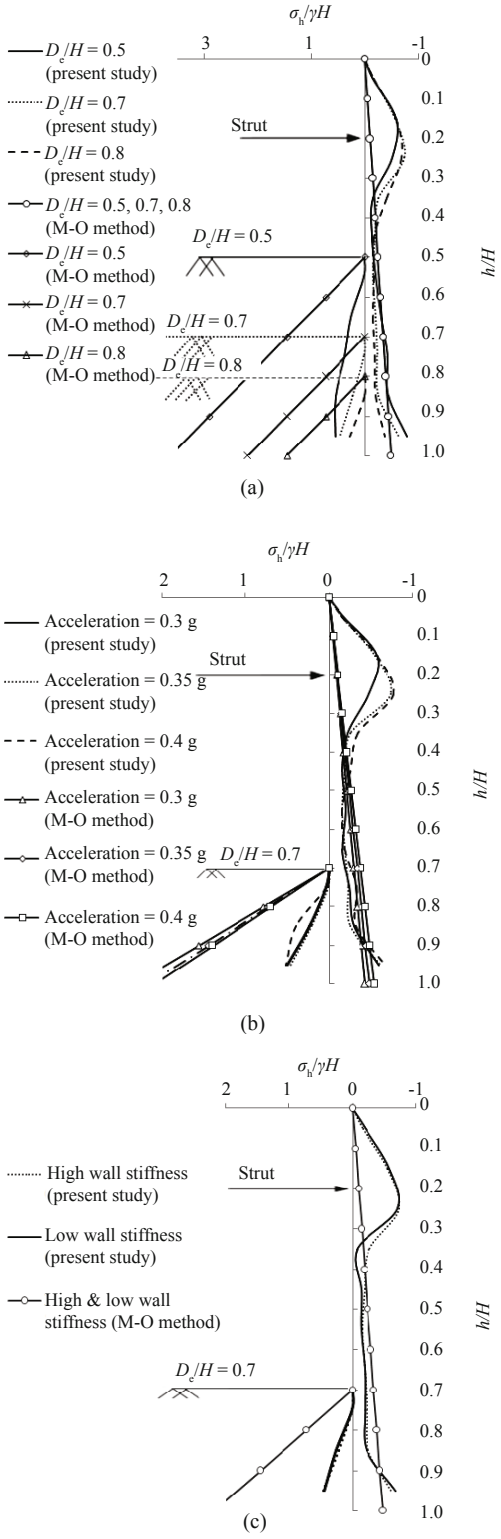

Fig. 11 Distribution of active and passive earth pressures behind the braced wall for (a) different excavation depths (D_e/H), (b) different peak amplitudes of input acceleration and (c) different wall stiffnesses

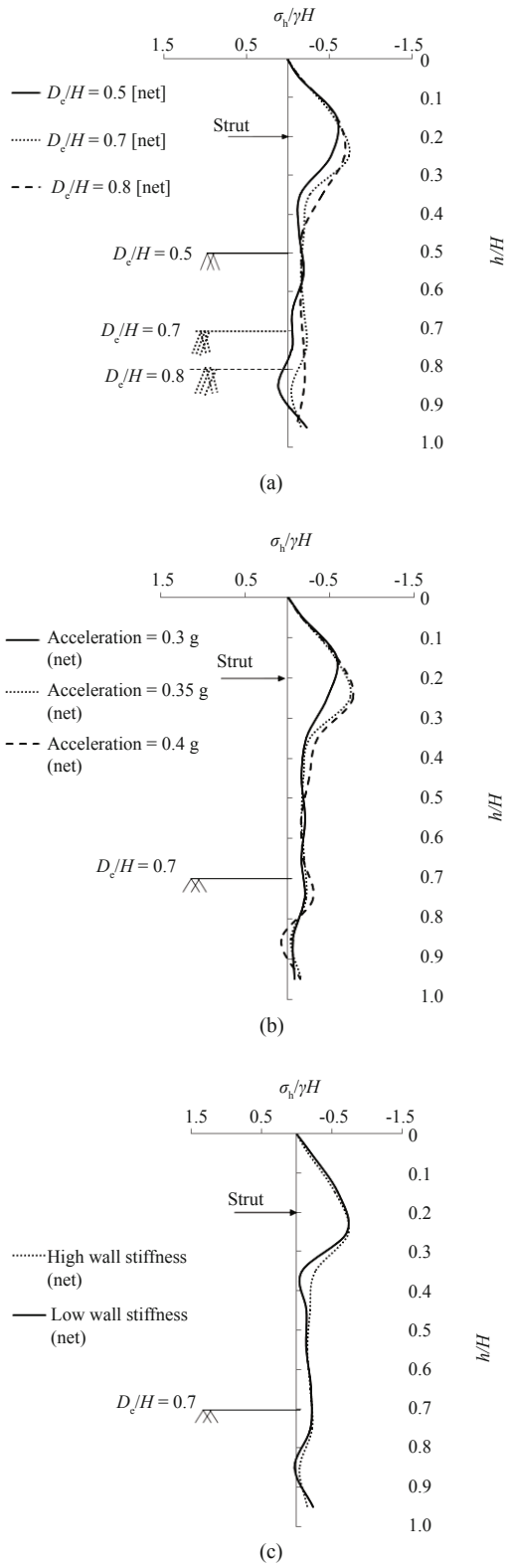

Fig. 12 Distribution of net earth pressure for different (a) excavation depths (D_e/H), (b) peak amplitudes of input acceleration and (c) wall stiffnesses

excavation level that was obtained from the numerical study. The difference between the passive earth pressure obtained from the theoretical method and the numerical study increased as the depth of the wall increased below the excavation level. For all cases, the maximum net lateral pressure was observed to act near strut levels. Thus, under a seismic condition for a single-strut case, the maximum net lateral earth pressure acted at the strut level, while for the multi-strut case, the net lateral earth pressure above the excavation level was fairly uniform due to the presence of more struts (as shown in Fig. 10).

5 Conclusions

Shake table tests and corresponding numerical analyses were performed on a single-strutted braced excavation, keeping the material properties, location of the struts and the width of the excavation identical for all cases. The experimental approach showed that when the amplitude of the base acceleration and the wall stiffness were kept constant, the lateral displacement, bending moments, strut forces and maximum ground surface displacement increased with the increment of the excavation depth (D_e/H). When the excavation depth (D_e/H) and the wall stiffness (EA) were kept constant, the lateral displacement, bending moments, strut forces and the maximum ground surface displacement increased with the peak amplitude of the input base acceleration. For a constant excavation depth (D_e/H) and peak acceleration amplitude, as wall stiffness decreased, the lateral displacement increased, bending moments in the wall decreased, strut forces decreased and ground surface displacement increased. As the excavation depth increased, maximum lateral displacement occurred near the bottom of the excavation.

The numerical study showed that—for the selected parameters—when the wall stiffness was decreased by 80%, the maximum value of u/D_e increased by around 60%, normalized strut force decreased by 7%, the maximum value of $M/\gamma H^3$ decreased by 26 % and the v/H value increased by 66%,. Thus, under a seismic condition, the change in the wall stiffness influenced deflection, the moment of the wall and ground surface displacement more when compared to the strut force. A uniform lateral displacement was observed within the excavated portion for the wall with higher stiffness. However, in the case of the wall with lower stiffness, more displacement was observed near the bottom of the excavation. From the numerical study, it is observed that—for the selected parameters—the maximum value of u/D_e increased by around 45%, normalized strut force increased by 8%, the maximum value of $M/\gamma H^3$ increased by 14% and the v/H value increased by 64%, when the peak acceleration increased from 0.35 g to 0.4 g. Thus, the lateral displacement of the wall and ground surface settlement were more affected than the bending moment in the wall and strut force due to the change in the peak acceleration applied at the base. Thus, strut force was the least affected parameter compared with the others under a seismic condition.

Coulomb's theory and the Mononobe-Okabe method underestimated the active lateral earth pressure

when compared to the active earth pressure near the strut level obtained from the numerical study for both the static and seismic conditions, respectively. However, the Mononobe-Okabe method overestimated the passive earth pressure when compared to the earth pressure throughout the depth of the wall below the excavation level that was obtained from the numerical study. The method proposed by Peck *et al*. (1974) for multi-propped excavations in sandy soil overestimated the lateral earth pressure for a static condition that was obtained by theoretical methods as well as numerical study. However, the earth pressure obtained from the numerical study under a seismic condition was more than the earth pressure proposed by Peck *et al*. (1974). Under a seismic condition, the earth pressure was greater near the strut level in the single-strut case, but, for the multi-strut case, the earth pressure was fairly uniform throughout the excavation depth (except near ground level). The uniform seismic earth pressure obtained by the numerical study (with an acceleration amplitude of 0.35 g) for the multi-strut case was almost three times more than the uniform earth pressure proposed by Peck *et al*. (1974). The net earth pressure behind the walls increased as the peak acceleration amplitude increased, but did not significantly change with the wall stiffness.

References

Atik LA and Sitar N (2010), "Seismic Earth Pressures on Cantilever Retaining Structures," *Journal of Geotechnical and Geoenvironmental Engineering*, **136**(10): 1324–1333.

Boscardin MD and Cording EJ (1989), "Building Response to Excavation–Induced Settlement," *Journal of Geotechnical Engineering*, ASCE, **115**(1): 1–21.

Bose SK and Som NN (1998), "Parametric Study of a Braced Cut by Finite Element Method," *Computers and Geotechnics*, **22**(2): 91–107.

Callisto L (2014), "Capacity Design of Embedded Retaining Structures," *Geotechnique*, **64**(3): 204–214

Callisto L, Soccodato FB and Conti R (2008), "Analysis of the Seismic Behavior of Propped Retaining Structures," *Proceedings of Geotechnical Earthquake Engineering and Soil Dynamics IV conference*, GSP 181, Sacramento, USA: 1–10.

Callisto L and Soccodato FM (2007), "Seismic Analysis of an Embedded Retaining Structure in Coarse Grained Soils," *Proceeding of the fourth international conference on earthquake geotechnical engineering*, Thessaloniki, Dordrecht, the Netherlands: Springer.

Callisto L and Soccodato FM (2009), "Performance-Based Design of Embedded Retaining Walls Subjected to Seismic Loading," *E. Cosenza (ed), Eurocode 8 Perspectives from the Italian Standpoint Workshop*, Doppiavoce, Napoli, Italy: 291–300.

Callisto L and Soccodato FM (2010), "Seismic Design of Flexible Cantilever Retaining Walls," *Journal of Geotechnical and Geoenvironmental Engineering*, **136**(2): 344–354.

Caltabiano S, Cascone E and Maugeri M (2000), "Seismic Stability of Retaining Walls with Surcharge," *Soil Dynamics and Earthquake Engineering*, **20**(8): 469–476.

Carrubba P and Colonna P (2000), "A Comparison of Numerical Methods for Multi-Tied Walls," *Computers and Geotechnics*, **27**(2): 117–140.

Chowdhury SS, Deb K and Sengupta A (2013), "Estimation of Design Parameters for Braced Excavation: A Numerical Study," *International Journal of Geomechanics*, ASCE, 13(3): 234–247.

Chowdhury SS, Deb K and Sengupta A (2015), "Behavior of Underground Strutted Retaining Structure under Seismic Condition," *Earthquakes and Structures*, **8**(5): 1147–1170.

Chowdhury SS, Deb K and Sengupta A (2016), "Effect of Fines on Behavior of Braced Excavation in Sand: Experimental and Numerical Study," *International Journal of Geomechanics*, ASCE, **16**(1): 04015018-1-13.

Conti R, Madabhushi GSP and Viggiani MB (2012), "On the Behavior of Flexible Retaining Walls under Seismic Action," *Geotechnique*, **62**(12): 1081–1094.

Conti R, Viggiani GMB and Madabhusi SPG (2010), "Physical Modeling of Flexible Retaining Walls under Seismic Actions," *Physical Modelling in Geotechnics*, Springman, Laue & Seward (eds), Taylor & Francis Group, London, ISBN 978-0-415-59288-8.

Costa P A, Borges JL and Fernandes MM (2007), "Analysis of a Braced Excavation in Soft Soils Considering the Consolidation Effect," *Journal of Geotechnical and Geological Engineering*, **25**: 617–629.

Day RA and Potts DM (1993), "Modeling Sheet Pile Retaining Walls," *Computers and Geotechnics*, **15**(3): 125–143.

Gazetas G, Psarropoulos PN, Anastasopoulos I and Gerolymos N (2004), "Seismic Behavior of Flexible Retaining Systems Subjected to Short-Duration Moderately Strong Excitation," *Soil Dynamics and Earthquake Engineering*, **24**(7): 537–550.

Georgiadis M and Anagnostopoulos C (1999), "Displacement of Structures Adjacent to Cantilever Sheet Pile Walls," *Soils and Foundations*, **39**(2): 99–104.

Finno RJ, Harahap IS and Sabatini PJM (1991), "Analysis of Braced Excavations with Coupled Finite Element Formulations," *Computers and Geotechnics*, **12**(2): 91–114.

Finno RJ and Harahap IS (1991), "Finite Element Analysis of HDR-4 Excavation," *Journal of Geotechnical Engineering Division*, **117**(10): 1590–1609.

Finno R, Arboleda-Monsalve L, and Sarabia F (2015), "Observed Performance of the One Museum Park West Excavation," *Journal of Geotechnical and Geoenvironmental Engineering*, ASCE, **141**(1): 04014078.

His JP and Small JC (1993), "Application of a Fully Coupled Method to the Analysis of an Excavation," *Soils and Foundations*, **33**(4): 36–48.

Hsieh PG, Ou CY and Lin YL (2013), "Three-Dimensional Numerical Analysis of Deep Excavations with Cross Walls," *Acta Geotechnica*, **8**(1): 33–48.

Hsieh PG and Ou CY (1998), "Shape of Ground Surface Settlement Profiles Caused by Excavation," *Canadian Geotechnical Journal*, **35**: 1004–1117.

Hsiung BCB (2009), "A Case Study on the Behavior of a Deep Excavation in Sand," *Computers and Geotechnics*, **36**(4): 665–675.

Itasca (2005), "FLAC Fast Lagrangian Analysis of Continua," v. 5.0, User's Manual.

Janbu N (1963), "Soil Compressibility as Determined by Oedometer and Triaxial Tests," *European Conference on Soil Mechanics & Foundation Engineering*, Wiesbaden, Germany, **1**: 19–25.

Karlsrud K and Andresen L (2005), "Loads on Braced Excavation in Soft Clay," *International Journal of Geomechanics*, **5**(2): 107–113.

Kung GTC, Juang CH, Hsiao ECL and Hashash YMA (2007), "Simplified Model for Wall Deflection and Ground-Surface Settlement Caused by Braced Excavation in Clays," *Journal of Geotechnical and Geoenvironmental Engineering*, **133**(6): 731–747.

Lombardi D, Bhattacharya S, Scarpa F and Bianchi M (2015), "Dynamic Response of a Geotechnical Rigid Model Container with Absorbing Boundaries," *Soil Dynamics and Earthquake Engineering*, **69**: 46–56.

Ling HI, Mohri Y, Leshchinsky D, Burke C, Matsushima K and Liu H (2005a), "Large Scale Shaking Table Tests on Modular Block-Reinforced Soil Retaining Walls," *Journal of Geotechnical and Geoenvironmental Engineering*, **131**(4): 465–476.

Ling HI, Liu H and Mohri Y (2005b), "Parametric Studies on the Behavior of Reinforced Soil Retaining Walls under Earthquake Loading," *Journal of Engineering Mechanics*, **131**(10): 1056–1065.

Ling HI, Leshchinsky D, Wang JP, Mohri Y and Rosen A (2009), "Seismic Response of Geocell Retaining Walls: Experimental Studies," *Journal of Geotechnical and Geoenvironmental Engineering*, **135**(4): 515–524.

Liu GB, Ng CWW and Wang ZW (2005), "Observed Performance of a Deep Multi-Strutted Excavation in Shanghai Soft Clays," *Journal of Geotechnical and Geoenvironmental Engineering*, **131**(8): 1004–1013.

Long M (2001), "Database for Retaining Wall and Ground Movements due to Deep Excavations," *Journal of Geotechnical and Geoenvironmental Engineering*, **127**(3): 203–224.

Madabhushi SPG and Zeng X (1998), "Seismic Response of Gravity Quay Walls. I: Numerical Modeling," *Journal of Geotechnical and Geoenvironmental Engineering*, **124**(5): 418–427.

Madabhushi SPG and Zeng X (2008), "Simulating Seismic Response of Cantilever Retaining Walls," *Journal of Geotechnical and Geoenvironmental Engineering*, **133**(5): 539–549.

Moormann C (2004), "Analysis of Wall and Ground Movements due to Deep Excavations in Soft Soil Based on a new worldwide database," *Soils and Foundations*, **44**(1): 87–98.

Nakai T, Kawano H, Murata K, Banno M and Hashimoto T (1999), "Model Test and Numerical Simulation of Braced Excavation in Sandy Ground: Influences of Construction History, Wall Friction, Wall Stiffness, Strut Position and Strut Stiffness," *Soils and Foundations*, **39**(3): 1–12.

Neelakantan G, Budhu M and Jr. Richards R (1992), "Balanced Seismic Design of Anchored Retaining Walls," *Journal of Geotechnical Engineering Division*, **118**(6): 873–888.

Ng CWW, Simpson B, Lings ML and Nash DFT (1998), "Numerical Analysis of a Multipropped Retaining Wall in Stiff Clay," *Canadian Geotechnical Journal*, **35**(1): 115–130.

Ou CY and Hsieh PG (2011), "A Simplified Method for Predicting Ground Settlement Profiles Induced by Excavation in Soft Clay," *Computers and Geotechnics*, **38**(8): 987–997.

Peck RB, Hanson WE and Thornburn TH (1974), *Foundation Engineering*, John Wiley & Sons, 514.

Psarropoulos PN, Klonaris G and Gazetas G (2005), "Seismic Earth Pressures on Rigid and Flexible Retaining Walls," *Soil Dynamics and Earthquake Engineering*, **25**(10): 795–809.

Richards Jr. R, Huang M and Fishman KL (1999), "Seismic Earth Pressure on Retaining Structures," *Journal of Geotechnical and Geoenvironmental Engineering*, **125**(9): 771–778.

Siller TJ and Frawley DD (1992), "Seismic Response of Multianchored Retaining Walls," *Journal of Geotechnical and Geoenvironmental Engineering*, **118**(11): 1787–1803.

Takemura J, Kondoh M, Esaki T Kouda M and Kusakabe O (1999), "Centrifuge Model Tests on Double Propped Wall Excavation in Soft Clay," *Soils and Foundations*, **39**(3): 75–87.

Tan Y, and Wang D (2013a), "Characteristics of a Large-Scale Deep Foundation Pit Excavated by the Central-Island Technique in Shanghai Soft Clay. I: Bottom-Up Construction of the Central Cylindrical Shaft," *Journal of Geotechnical and Geoenvironmental Engineering*, ASCE, **139**(11): 1875–1893.

Tan Y and Wang D (2013b), "Characteristics of a Large-Scale Deep Foundation Pit Excavated by the Central-Island Technique in Shanghai Soft Clay. II: Top-Down Construction of the Peripheral Rectangular Pit," *Journal of Geotechnical and Geoenvironmental Engineering*, ASCE, **139**(11): 1894–1910.

Tanaka H (1999), "Behavior of a Braced Excavation in Soft Clay and the Undrained Shear Strength for Passive Earth Pressure," *Soils and Foundations*, **34**(1): 53–64.

Tefera TH, Nordal S, Grande L, Sandven R and Emdal A (2006), "Ground Settlement and Wall Deformation from a Large Scale Model Test on as Single Strutted Sheet Pile Wall in Sand," *International Journal of Physical Modelling in Geotechnics*, **2**: 1–13.

Tufenkjian MR and Vucetic M (2000), "Dynamic Failure Mechanism of Soil-Nailed Excavation Models in Centrifuge," *Journal of Geotechnical and Geoenvironmental Engineering*, **126**(3): 227–235.

Veiskarami M, Bahar A and Lak EZ (2015), "Dynamic Earth Pressure on Rigid Retaining Walls Induced by a Neighboring Machine Foundation, by the Meshless Local Petrov-Galerkin Method," *Earthquake Engineering and Engineering Vibration*, **14**(4): 647–661

Wang ZW, Ng CWW and Liu GB (2005), "Characteristics of Wall Deflections and Ground Surface Settlements in Shanghai," *Canadian Geotechnical Journal*, **42**(5): 1243–1254.

Wang JH, Xu ZH and Wang WD (2010), "Wall and Ground Movements due to Deep Excavations in Shanghai Soft Soils," *Journal of Geotechnical and Geoenvironmental Engineering*, **136**(7): 985–994.

Wartman J, Rondinel-Oviedo, EA and Rodriguez-Marek A (2006), "Performance and Analyses of Mechanically Stabilized Earth Walls in the Tecoman, Mexico Earthquake," *Journal of Performance of Constructed Facilities*, **20**(3): 287–299.

Watanabe K, Munaf Y, Koseki J, Tateyama M and Kojima K (2003), "Behaviors of Several Types of Model Retaining Walls Subjected to Irregular Excitation," *Soils and Foundations*, **43**(5): 13–27.

Whittle A J, Corral G, Jen L C, and Rawnsley RP (2015), "Prediction and Performance of Deep Excavations for Courthouse Station, Boston." *Journal of Geotechnical and Geoenvironmental Engineering*, ASCE, **141**(4): 04014123.

Yogendrakumar M, Bathurst RJ and Finn WDL (1992), "Dynamic Response Analysis of Reinforced Soil Retaining Wall," *Journal of Geotechnical and Geoenvironmental Engineering*, **118**(8): 1158–1167.

Yoo C and Lee D (2008), "Deep Excavation-Induced Ground Surface Movement Characteristics – A Numerical Investigation," *Computers and Geotechnics*, **35**(2): 231–252.

Zdravkovic L, Potts DM and St. John HD (2005), "Modeling of a 3D Excavation in Finite Element Analysis," *Geotechnique*, **55**(7): 497–513.

Zeng X (1998), "Seismic Response of Gravity Quay Walls. I: Centrifuge Modeling," *Journal of Geotechnical and Geoenvironmental Engineering*, **124**(5): 406–417.

Notation

The following symbols are used in this paper:

A = cross-sectional area of strut
B = width of excavation
c' = effective cohesion
c_u = uniformity coefficient
c_c = coefficient of curvature
D_e = excavation depth
D_b = embedded depth
E = Young's modulus of plexiglass
E_p = Young's modulus of plexiglass (plane strain)
E_s = Young's modulus of soil
F = axial force in strut
G = shear modulus of soil
h = distance from top ground surface
H = total height of the wall
I = moment of inertia
K = bulk modulus of soil
K_h = coefficient of lateral earth pressure
K_n = interface normal stiffness between wall and soil
K_s = interface shear stiffness between wall and soil
M = bending moment in wall
s = distance of the struts from top
t_w = thickness of wall
u = horizontal wall displacement
v = vertical ground displacement
ϕ' = effective angle of internal friction
Ψ = dilation angle of soil
μ_s = Poisson's ratio of soil
γ = unit weight of the soil
x = distance from wall
Z = total soil depth